Applied Physics Letters ARTICLE scitation.org/journal/apl

Stimulated emission in vicinity of the critical angle

Cite as: Appl. Phys. Lett. **119**, 031102 (2021); doi: 10.1063/5.0051901
Submitted: 28 March 2021 · Accepted: 5 July 2021 ·
Published Online: 19 July 2021

Joshua K. Asane,[1] Md G. R. Chowdhury,[1] Kanij M. Khabir,[1] Viktor A. Podolskiy,[2] and Mikhail A. Noginov[1,a)]

AFFILIATIONS

[1]Center for Materials Research, Norfolk State University, Norfolk, Virginia 23504, USA
[2]Department of Physics and Applied Physics, University of Massachusetts, Lowell, Massachusetts 01854, USA

Note: This Paper is part of the APL Special Collection on Metastructures: From Physics to Applications.
[a)]**Author to whom correspondence should be addressed:** mnoginov@nsu.edu

ABSTRACT

We have demonstrated amplified spontaneous emission (ASE) propagating along the planar interface between two adjacent dielectrics with slightly different refractive indexes. This emission originates from the leaky mode, fueled by optical gain in the low-index dielectric, that is outcoupled to the high-index dielectric in vicinity of the critical angle for total internal reflection. This led us to the observation of spectacular concentric rings of ASE emission occurring above the low and soft stimulated emission threshold. The results of our study can be used to develop novel miniature low-threshold stimulated emission sources and photonic circuits operating at optical frequencies.

To keep up with the Moore's law,[1] predicting computers' capability to double every two years, future electronics will need nanocircuits operating at optical frequencies.[2] This novel technology will require optical analogs of resistors, capacitors, inductances, as well as oscillators and amplifiers. Historically, the development of passive nanocircuit elements was followed by the development of more complicated active components with gain, such as (metal-based) plasmonic nanolasers and spasers.[3–5] While the latter provide the compactness required of photonic nanocircuitry, plasmonic lasers (and spasers) suffer from inherent optical loss in metal. Therefore, the development of metal-free miniature lasers with the functionality similar to plasmonic lasers, but without high loss, would be a major breakthrough in the development of photonic circuitry.

In the present study, we consider the geometry depicted in Fig. 1 (low index dielectric with gain adjacent to a higher index dielectric without gain) and investigate (i) whether an amplified spontaneous emission (ASE) wave can be supported by low-index dielectric layers and (ii) whether it can support low-loss stimulated emission.

Similar configurations were theoretically and experimentally studied by several authors[6–14] and shown to have the total internal reflection exceeding unity, with the maximum at or slightly below the critical angle. The latter amplification of the reflected light (also predicted in our calculations) was due to the interaction of propagating or evanescent waves (occurring in vicinity of the critical angle) with the optical gain in the low-index medium.

However, the primary interest of the present study is not an amplification of the reflected light, but rather the generation of guided stimulated emission in low-index dye-doped polymer adjacent to the high-index glass. Lasers and ASE sources, harvesting optical gain with evanescent fields, have been reported in the literature in planar[6,15] and cyllindrical geomerties.[16–18]

Here, we report a proof-of-principle demonstration of a miniature all-dielectric source of stimulated emission, directly out-coupled into a guided mode of a planar glass slab, and explain the observed behavior analytically and numerically. The demonstrated all-dielectric ASE sources, when properly coupled to photonic circuitry, may be suitable for micrometer scale on-chip applications.

Our experimental samples were polymeric films (PMMA) doped with rhodamine 6G (R6G) dye (gain medium) deposited onto soda-lime glass substrates [Fig. 1(a)]. The R6G:PMMA film thickness ranged between $l_{PMMA} = 1.68\ \mu$m and $l_{PMMA} = 4.15\ \mu$m, and the dye concentrations ranged from $c = 5$ g/l to 400 g/l (in solid state, when the solvent evaporated). The fabrication and characterization of the R6G:PMMA films are described in detail in Refs. 19 and 20. At the wavelength $\lambda = 575$ nm, which was close to the wavelength of maximal emission of R6G $\lambda = 563$ nm, the refractive indexes of glass and (undoped) PMMA are $n_{glass} = 1.5239$[21] and $n_{PMMA} = 1.4912$,[22] respectively. [We will refer to them as *high index dielectric (glass)* and *low index dielectric (PMMA)*, although the two refractive indices are very close to each other.]

The samples described above were optically pumped at $\lambda = 532$ nm with a frequency doubled Q-switched Nd:YAG laser, $t_{pulse} \sim 10$ ns, at 57° to the sample's normal (Fig. 2). The pumped spot was nearly elliptical, with the long axis, determined using the knife-edge

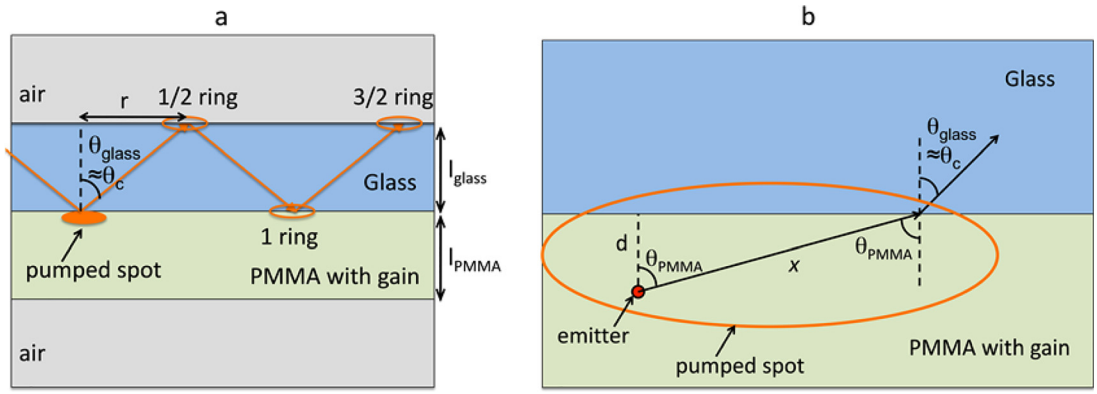

FIG. 1. (a) Sample geometry and the model of light propagation: amplified spontaneous emission (ASE) in the pumped spot gets outcoupled from PMMA to glass at the angle close to the critical angle θ_c and then propagates in the glass + PMMA pair of layers, being supported by reflections at the glass/air, glass/PMMA, and PMMA/air interfaces (not shown). (b) Zoomed pumped spot in (a) (not in scale).

technique, equal to ~8 mm. The area of the pumped spot was ~27 mm^2. The emission, with the maximum at $\lambda = 563$ nm [Fig. 3(a)], was detected at 33° to the sample's normal, using a focusing lens, a monochromator, a photomultiplier tube (photodetector), signal processing electronics, and a computer (Fig. 2).

When the sample, the R6G:PMMA film ($l_{PMMA} = 3.22\ \mu$m, c = 5 g/l) deposited onto a 1 mm glass slide, was pumped with low-energy pulses, <0.025 mJ, a weak spot of emission (partly mixed with the scattered pumping light) was seen on the sample [Figs. 3(a)–3(e)]. The emission spectral band had the full width at half maximum (FWHM) ranging between 34 nm and 40 nm [Fig. 3(c)].

With an increase in the pumping energy (0.065 mJ), the bright spot became larger and got surrounded by a diffused light [Fig. 3(f)].

At the further increase in the pumping energy (above the critical soft threshold of 0.14 mJ), a spectacular bright ring, followed by several other concentric rings appeared on the sample's surface [Figs. 3(g) and 3(h)]. We denoted these bright rings with integer numbers m = 1, 2, 3…etc. Much less intense and often discontinuous emission rings could be seen in between the major "integer" emission rings, see the arrow in Fig. 3(h). We numerated the latter low intensity rings as m = 1/2, 3/2, 5/2, …, etc.

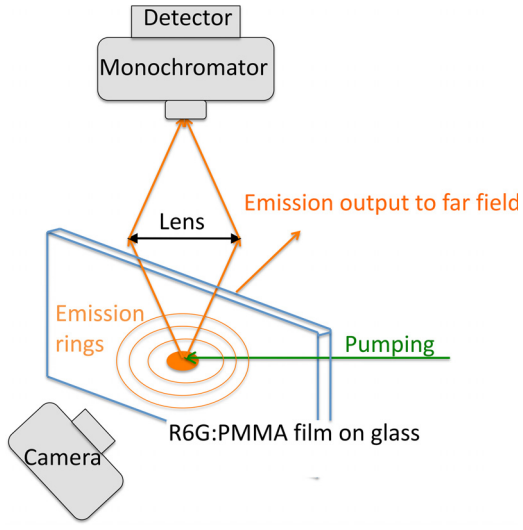

FIG. 2. Experimental setup: Sample with emission rings, focusing lens, monochromator, photodetector, and photo camera.

The rings seemed to originate from scattering of light, otherwise guided by the glass + PMMA pair of layers [Fig. 1(a)], by unintentional surface and volume imperfections in R6G:PMMA (stronger effect) and glass (weaker, primarily surface, effect). No rings of light could be intercepted by a white card placed next to the sample's surface. However, an arched trace of light could be seen on a white card placed above the sample, suggesting that the emitted light was guided by the glass + polymer structure toward its edge (guided mode) (Fig. 2). The rings did not disappear when an electrical black tape was adhered to the glass, from the side opposite to the R6G:PMMA film. The qualitatively similar patterns were observed when the R6G:PMMA film was facing the pumping laser and the monochromator or when the sample was flipped and an uncoated glass was facing both the pumping beam and the monochromator.

The onset of the emission ring corresponded to the reduction in the emission bandwidth, down to FWHM = 24 nm [Figs. 3(a) and 3(c)], and an increase in the emission intensity [Fig. 3(b)]. Note that the horizontal axes in Figs. 3(b) and 3(c) show the logarithm of the pumping energy. If the horizontal axis was made to be linear, the plot of intensity *vs* pumping would demonstrate a growth with saturation. Note that in this particular experiment, we collected and analyzed the scattered light rather than the light guided by the glass and the R6G:PMMA film.

When the dye doped PMMA films were deposited onto a 1 mm thick glass slide, the radii of integer and semi-integer rings grew linearly with the increase in the ring number [Fig. 4(a)], following the formula $r = m \times 10.76$ mm (at the film thickness equal to $l_{PMMA} = 3.22\ \mu$m). Assuming that light is guided by the glass slide as shown in Fig. 1(a), the angle of light propagation is equal to $\theta_{glass} = \text{arctg}(10.76/2) = 79.47°$, which is close to the critical angle at the glass/PMMA interface, $\theta_c = \text{asin}(n_{PMMA}/n_{glass}) = 78.11°$. (Note that both the experimental angle θ_{glass} and the calculated critical angle

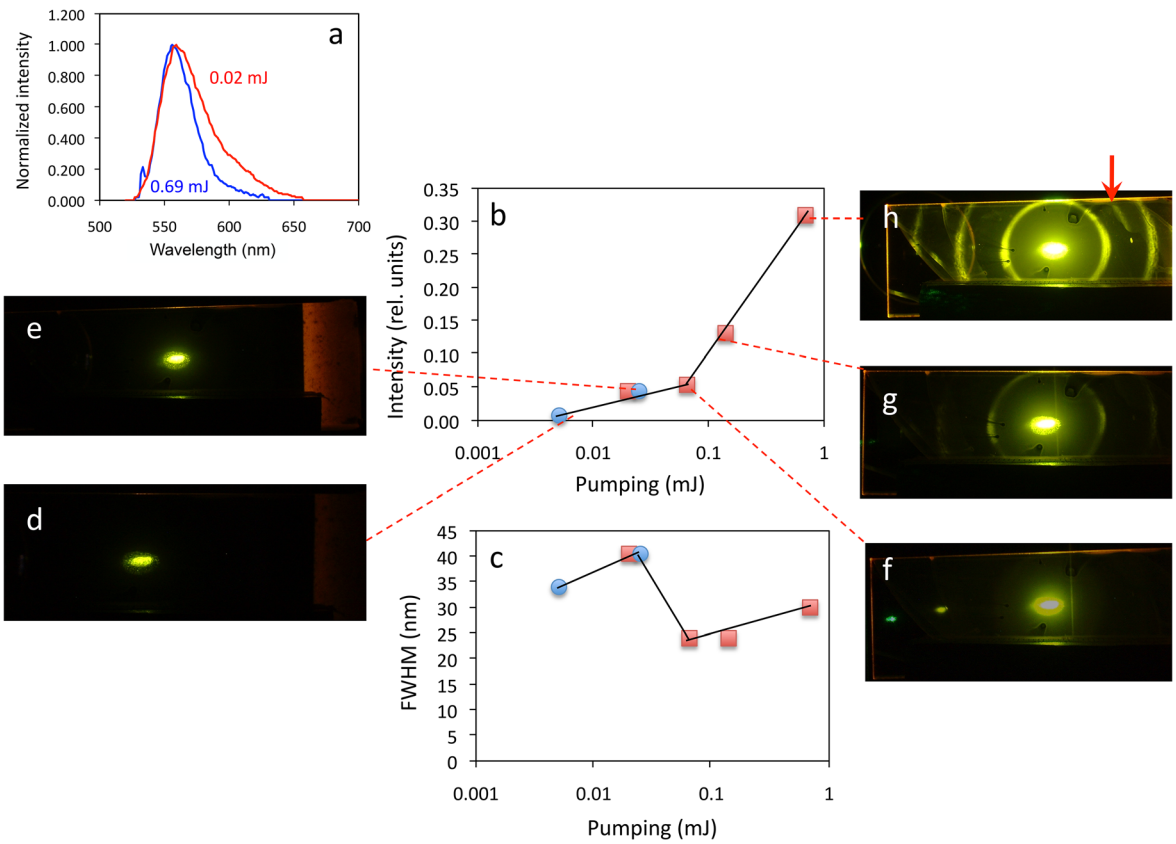

FIG. 3. (a) Emission spectra of R6G:PMMA (normalized to unity) measured at pumping energy of 0.02 mJ (red trace) and 0.69 mJ (blue trace). (b) Emission intensity plotted against pumping energy. (c) Full width at half maximum (FWHM) plotted against pumping energy. [(d)–(h)] Photographs of the emission patterns taken at pumping energies equal to 0.0051, 0.025, 0.065, 0.14, and 0.69 mJ, respectively.

θ_c are known with the accuracy $\pm 1°$.) In agreement with the same model of light propagation depicted in Fig. 1(a), the ring diameter linearly increased with an increase in the thickness of the glass slide [Fig. 4(b)]. [In this particular experiment, one of the slides was made of poly (vinyl chloride) (PVC), whose refractive index, $n_{PVC} = 1.531$ (at 589 nm),[23] was very close to that of the soda-lime glass.] At the same time, the ring diameter was nearly independent of the thickness of the R6G:PMMA film [Fig. 4(c)]. It also did not depend on the pumping intensity (not shown). When the emission pattern was photographed through the long-pass color filter transmitting light at $\lambda > 590$ nm, orange emission dominated the image. However, the radii of the rings remained to be unchanged [Fig. 4(d)].

The soft ASE threshold is observed in the studied all-dielectric geometry at the pumping energy density equal to $E_{th}/S = 0.24$ mJ/cm^2 ($E_{th} = 0.065$ mJ and $S = 0.27$ cm^2), see Figs. 4(b) and 4(g). This value is nearly ten times smaller than the threshold of stimulated emission of surface plasmon polaritons (SPP) with the gain of 2.18 mJ/cm^2 (Ref. 4) in a fair agreement with the theoretical estimates below. This paves the way to on-chip realization of low-loss all-dielectric stimulated emission sources.

Note that the qualitatively similar rings were observed at the R6G concentration equal to $c = 10$ g/l. However, no rings have been seen at higher R6G concentrations or when the Rhodamine B (RhB) dye was used instead of R6G dye. This behavior is the subject of further studies to be published elsewhere.

Several theoretical and numerical studies have been performed to understand the observed phenomenon. The first of these analyzed the propagation of the (leaky) modes supported by the multilayered stack that is formed by high-index glass substrate, low-index PMMA guiding layer, and air cladding [Figs. 5(a) and 5(b)]. Since the propagation constant of these leaky modes is within the light cone in the high-index glass substrate, this constant can be mapped to the escape angle of the mode via

$$k_x = n_{PMMA}\omega \sin\theta/c. \quad (1)$$

Note that this escape angle is very close to the critical angle at glass/PMMA interface. As seen in the figure, the propagation length of these modes is controlled by the level of gain in PMMA layer and PMMA layer thickness. The increase in gain (or thickness) of the layer yields an increase in the propagation length. When the PMMA gain reaches the (thickness-dependent) critical gain level, stimulated emission compensates the leakage loss, leading to the onset of ASE, observed in our experiment. Importantly, when PMMA thickness is larger than ~ 1.5 μm, the critical gain required to overcome the radiation losses in all-dielectric systems is smaller than the one required to overcome

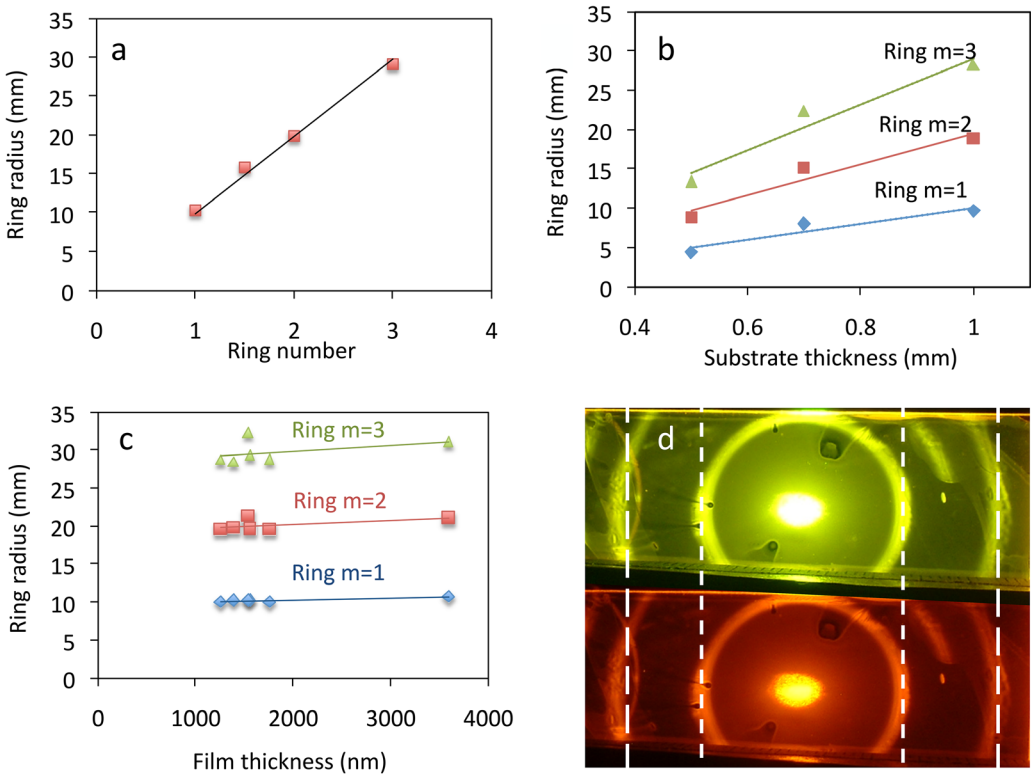

FIG. 4. (a) Dependence of the ring's radius on the ring's number m. (b) Dependence of the ring's radius on the thickness of the substrate (plotted for rings m = 1, m = 2, and m = 3). (c) Dependence of the ring's radius on the thickness of the R6G:PMMA film (plotted for rings m = 1, m = 2, and m = 3). (d) Emission rings photographed without filter (top) and with 590 nm long-pass filter (bottom). One can see that the size of the ring does not depend on the color of emission.

propagation losses of an SPP propagating on silver/PMMA interface. This result is in agreement with our experimental studies.

In a separate set of studies, we utilized Green's function formalism[24,25] to analyze the emission of the dipolar sources embedded into a (otherwise passive) PMMA layer. The results of these calculations are shown in Fig. 5(c). Note that the angular position of the emission maximum matches the propagation constant of the leaky mode, once again indicating that the experimentally observed ASE results from the coupling of the emitted light into leaky waveguide modes. The fully coherent wave solutions of Maxwell equations, reported above, are also consistent with the following intuitive geometrical optics approach.

Let us assume that a point source of photons, which emits uniformly in 4π solid angle and whose trajectories are represented by rays of light, is located, as shown in Fig. 1(b), in vicinity of an interface between two dielectric media, R6G:PMMA with optical gain g and small index n_1 and glass with a larger index n_2 and no gain. (Here and

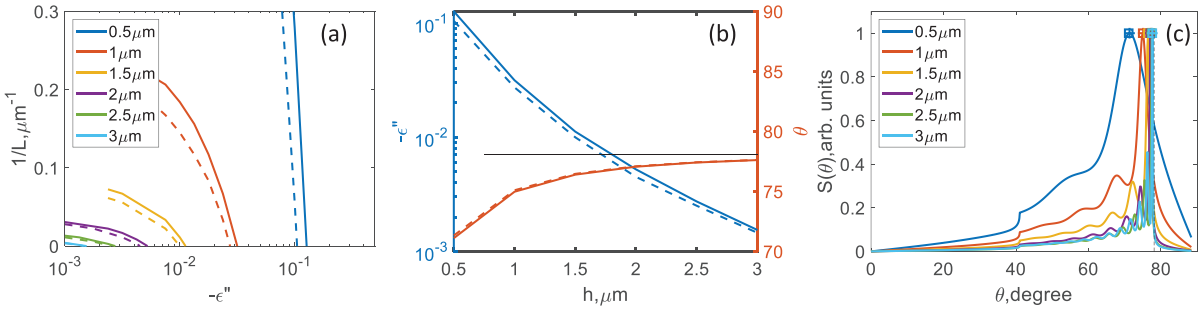

FIG. 5. (a) Dependence of the propagation length of the optical modes supported by the glass–PMMA–air stack on the gain in PMMA (parameterized via imaginary part of permittivity) for different PMMA thickness; (b) critical gain and the outcoupling angle of the modes in (a) as a function of PMMA thickness; in both (a) and (b) solid (dashed) lines represent TM and TE modes, respectively; thin black line in (b) represents critical angle at glass/PMMA interface; (c) angular profile of emission of the point dipole located within the glass/PMMA/air stacks; symbols represent outcoupling angles from (b). Numerical codes used to generate Fig. 5 are available online: https://github.com/viktor-podolskiy/Stimulated-emission-in-vicinity-of-the-critical-angle.

below, we will use subscript 1 for PMMA and subscript 2 for glass.) The beam depicted in Fig. 1(b) will propagate in the gain medium over distance

$$x = d/\cos\theta_1, \tag{2}$$

and get amplified by a factor $\exp(gx)$, where d is the distance to the interface and θ_1 is the incidence angle in PMMA. After that, the beam will get out-coupled to the glass at the angle θ_2 given by the Snell's law

$$\sin\theta_2 = (n_1/n_2)\sin\theta_1, \tag{3}$$

which we assume to be unaffected by the small gain g. The intensity of the outcoupled light in glass I_2 is given by

$$I_2 = I_1 \exp(gx)T, \tag{4}$$

where I_1 is the intensity of emitted light in PMMA (before amplification) and T is the Frensel's transmittance at the interface between PMMA and glass (which we also assume to be unaffected by gain g). The latter transmittance is given by the Frensel equations for s and p polarized light.[26]

The ratios I_2/I_1, calculated (in p polarization) for $g = 1000\,\mathrm{cm}^{-1}$ as functions of the refraction angle θ_2, are depicted in Fig. 6. One can see that the ratios are maximal at $\theta_2 \to \theta_c$ ($\theta_1 \to 90°$). This qualitative result is independent of the distance d, although the ratio I_2/I_1 grows exponentially with an increase in d. We, thus, have shown that in the geometry of Fig. 1, the spontaneous emission is amplified in R6G:PMMA, after which it gets outcoupled to glass. The amplification is particularly strong as θ_1 approaches 90° (gracing incidence) and, correspondingly, θ_2 approaches the critical angle. (Note that the gain saturation, which was not taken into account in our calculations, would reduce the calculated magnitudes of I_2/I_1 by orders of magnitude.)

In the geometry of our experiment, both R6G:PMMA and glass are not semi-infinite, but rather slabs of finite width, surrounded by air on both sides. Correspondingly, the amplified beam out-coupled from PMMA to glass is reflected (at the glass/air interface) in the direction of PMMA, where it is partly or fully reflected back at the glass/PMMA interface or PMMA/air interface. Each time when this guided light "touches" any of the interfaces or propagates through the polymeric film, part of it gets scattered by surface and volume imperfections (larger in polymer than in glass). In a planar sample geometry, emitted light radially propagates away from the pumped spot, leading to the formation of bright rings of ASE at large enough optical gain.

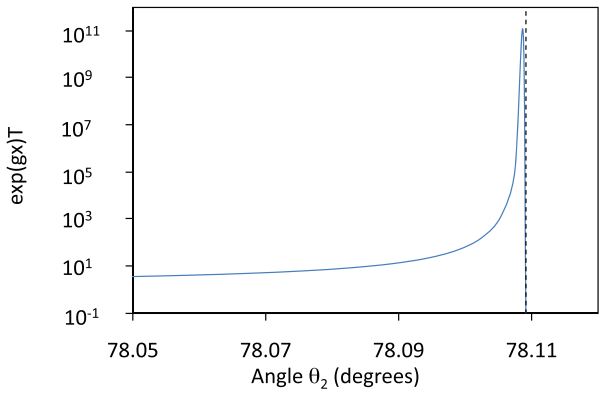

FIG. 6. Dependence of $\exp(gx)T$ on the outcoupling angle in glass (θ_2) in the geometry of Fig. 1(b). The distance d between the emission source and the interface is equal to 0.5 μm. Vertical dashed line corresponds to the critical angle θ_c.

In this model, we did not take in consideration (finite spatial) coherence of ASE emission, which possibly can explain the fact that widths of the rings are smaller than the size of the pumped spot. This is the subject of the future study to be published elsewhere.

To summarize, we have observed spectacular concentric rings of amplified spontaneous emission (ASE) propagating, above low and soft threshold, at the planar interface between two adjacent dielectric media with slightly different refractive indexes. This ASE wave, fueled by optical gain in the low-index dielectric medium, is outcoupled to the high-index dielectric medium in vicinity of the critical angle for total internal reflection. The observed phenomenon is explained analytically and numerically. The results of our study can be used to develop novel miniature low-threshold all-dielectric stimulated emission sources and photonic circuits operating at optical frequencies. When designing such practical active components, it is important to take into account the spatial mode profile in the presence of the evanescently coupled gain layer.

The authors acknowledged U.S. Department of Defense (No. W911NF1810472), Air Force Office of Scientific Research (No. FA9550-18-1-0417), and National Science Foundation (Nos. 1830886, 1856515, and 1629330).

DATA AVAILABILITY

The data that support the findings of this study are available from the corresponding author upon reasonable request. Numerical codes used to generate Fig. 5 are available online: https://github.com/viktor-podolskiy/Stimulated-emission-in-vicinity-of-the-critical-angle.

REFERENCES

[1]G. E. Moore, Electronics **57**(8), 114 (1965).
[2]N. Engheta, Science **317**(5845), 1698 (2007).
[3]D. J. Bergman and M. I. Stockman, Phys. Rev. Lett. **90**, 027402 (2003).
[4]M. A. Noginov, G. Zhu, M. Mayy, B. A. Ritzo, N. Noginova, and V. A. Podolskiy, Phys. Rev. Lett. **101**(22), 226806 (2008).
[5]M. A. Noginov, G. Zhu, A. M. Belgrave, R. Bakker, V. Suteewong, and U. Wiesner, Nature **460**, 1110 (2009).
[6]B. Ya Kogan, V. M. Volkov, and S. A. Lebedev, Pis'ma Zh. Eksp. Teor. Fiz. **16**, 144 (1972) [JETP Lett. **16**, 100 (1972)].
[7]G. N. Romanov and S. S. Shakhidzhanov, JETP Lett. **16**, 209 (1972).
[8]W. Lukosz and P. P. Herrmann, Opt. Commun. **17**, 192 (1976).
[9]P. R. Callary and C. K. Carniglia, J. Opt. Soc. Am. **66**, 775 (1976).
[10]R. F. Cybulski and C. K. Carniglia, J. Opt. Soc. Am. **67**, 1620 (1977).
[11]A. A. Kolokolov, JETP Lett. **21**, 312 (1975).
[12]R. F. Cybulski and M. P. Silverman, J. Opt. Soc. Am. **73**, 1732 (1983).
[13]J. Fan, A. Dogariu, and L. J. Wang, Opt. Express **11**, 299 (2003).
[14]K. J. Willis, J. B. Schneider, and S. C. Hagness, Opt. Express **16**, 1903 (2008).
[15]E. P. Ippen and C. V. Shank, Appl. Phys. Lett. **21**, 301 (1972).
[16]C. J. Koester, IEEE J. Quantum Electron. **2**, 580 (1966).
[17]Y.-X. Zhang, X.-Y. Pu, K. Zhu, and L. Feng, J. Opt. Soc. Am. B **28**, 2048 (2011).
[18]Y. Zhang, D. Li, Y. Ou, X. Pu, and Y. Sun, IEEE Photonics J. **11**, 1501709 (2019).
[19]E. K. Tanyi, H. Thuman, N. Brown, S. Koutsares, V. A. Podolskiy, and M. A. Noginov, Adv. Opt. Mater. **5**, 1600941 (2017).
[20]J. K. Asane and M. A. Noginov, J. Opt. Soc. Am. B **37**, 3108 (2020).

[21]R. V. Gibbons and T. J. Ahrens, J. Geophys. Res. **76**(23), 5489, https://doi.org/10.1029/JB076i023p05489 (1971).
[22]See M. N. Polyanskiy, https://refractiveindex.info for "Refractive Index Database;" accessed 6 October 2020.
[23]Vendor's specification, Thermo Fisher Scientific.
[24]S. R. J. Brueck, IEEE J. Sel. Top. Quantum Electron. **6**, 899 (2000).
[25]L. Nordin, K. Li, A. Briggs, E. Simmons, S. Bank, V. A. Podolskiy, and D. Wasserman, Appl. Phys. Lett. **116**, 021102 (2020).
[26]M. V. Klein and T. E. Furtak, *Optics* (John Wiley and Sons, New York, 1986).